Vision Research 49 (2009) 115–126

Contents lists available at ScienceDirect

Vision Research

journal homepage: www.elsevier.com/locate/visres

A computerized analysis of the entire retinal ganglion cell population and its spatial distribution in adult rats

M. Salinas-Navarro [a,1], S. Mayor-Torroglosa [a,1], M. Jiménez-López [a,1], M. Avilés-Trigueros [a], T.M. Holmes [b], R.D. Lund [c], M.P. Villegas-Pérez [a], M. Vidal-Sanz [a,*]

[a] Laboratorio de Oftalmología Experimental, Facultad de Medicina, Universidad de Murcia, E-30100 Murcia, Spain
[b] Catherine McCauley Centre, University College Dublin, Dublin, Ireland
[c] Casey Eye Institute, Oregon Health and Sciences University, Portland, OR, USA

ARTICLE INFO

Article history:
Received 25 June 2008
Received in revised form 12 September 2008

Keywords:
Retinal ganglion cells
Visual streak
Fluorescent tracers
Computerized image analysis
Retina
Rat
Retrograde labelling

ABSTRACT

In adult albino (SD) and pigmented (PVG) rats the entire population of retinal ganglion cells (RGCs) was quantified and their spatial distribution analyzed using a computerized technique. RGCs were back-labelled from the optic nerves (ON) or the superior colliculi (SCi) with Fluorogold (FG). Numbers of RGCs labelled from the ON [SD: 82,818 ± 3,949, $n = 27$; PVG: 89,241 ± 3,576, $n = 6$) were comparable to those labelled from the SCi [SD: 81,486 ± 4,340, $n = 37$; PVG: 87,229 ± 3,199; $n = 59$]. Detailed methodology to provide cell density information at small scales demonstrated the presence of a horizontal region in the dorsal retina with highest densities, resembling a visual streak.

1. Introduction

The retinofugal system of the adult rat has been used extensively as an experimental model to study anatomical, physiological and behavioural aspects of regeneration (Avilés-Trigueros, Sauvé, Lund, & Vidal-Sanz, 2000; Sasaki et al., 1996; Vidal-Sanz, Avilés-Trigueros, Whiteley, Sauvé, & Lund, 2002; Vidal-Sanz, Bray, Villegas-Pérez, Thanos, & Aguayo, 1987; Vidal-Sanz, Villegas-Pérez, Bray, & Aguayo, 1993; Whiteley, Sauvé, Avilés-Trigueros, Vidal-Sanz, & Lund, 1998), degeneration (Lafuente, Villegas-Pérez, et al., 2002; Lund et al., 2007; Villegas-Pérez, Lawrence, Vidal-Sanz, Lavail, & Lund, 1998; Villegas-Pérez, Vidal-Sanz, Bray, & Aguayo, 1988; Villegas-Pérez, Vidal-Sanz, & Lund, 1996; Villegas-Pérez, Vidal-Sanz, Rasminsky, Bray, & Aguayo, 1993) and neuroprotection (Avilés-Trigueros et al., 2003; Lafuente López-Herrera, Mayor-Torroglosa, Miralles de Imperial, Villegas-Pérez, & Vidal-Sanz, 2002; Lund et al., 2007; Mayor-Torroglosa et al., 2005; Vidal-Sanz, et al., 2000; Vidal-Sanz, De la Villa, et al., 2007) in the mammalian central nervous system. Indeed, the use of retrogradely transported neuronal tracers to identify the RGC population has allowed investigations into the effects of several types of injuries to the primary visual pathway and quantification of RGC survival (Lafuente, Villegas-Pérez, et al., 2002; Peinado-Ramón, Salvador, Villegas-Pérez, & Vidal-Sanz, 1996; Sellés-Navarro, Villegas-Pérez, Salvador-Silva, Ruiz-Gómez, & Vidal-Sanz, 1996). Moreover, orthogradely transported neuronal tracers have made it possible to identify not only fine retinofugal projections (Avilés-Trigueros et al., 2000), but also to quantify the volume of the retinotectal afferents to the contralateral visual layers of the superior colliculus (SC) in normal circumstances and after a lesion (Avilés-Trigueros et al., 2003; Mayor-Torroglosa et al., 2005).

Previous studies have indicated that a majority of RGCs project to the superior colliculi (SCi) (Lund, 1965; Perry, 1981) where RGCs axons deploy in a very precise topographic manner (Linden & Perry, 1983; Sauvé, Girman, Wang, Keegan, & Lund, 2002; Sauvé, Girman, Wang, Lawrence, & Lund, 2001), but to date the exact magnitude of this projection has not been quantified. The rat RGC population is distributed throughout the retina in a central-peripheral gradient and some authors have found a region with highest RGC density in the dorsal temporal retina (Dreher, Sefton, Ni, & Nisbett, 1985; Fukuda, 1977; Jeffery, 1985; McCall, Robinson, & Dreher, 1987; Perry, 1981; Reese & Cowey, 1986; Schober & Gruschka, 1977), but whether they adopt some form of regional specialization remains controversial (Danias et al., 2002; Reese, 2002). The Sprague–Dawley (SD) and Piebald Virol Glaxo (PVG) Brown Norway strains of rats with non-pigmented and pigmented eyes, respectively, are commonly employed for a number of experimental approaches aimed at studying injury-induced RGC loss and its prevention, thus it was of interest to determine, as a baseline for

* Corresponding author. Fax: +34 968 36 39 62.
E-mail address: ofmmv01@um.es (M. Vidal-Sanz).
[1] These authors have contributed equally towards this work.

0042-6989/$ - see front matter © 2008 Elsevier Ltd. All rights reserved.
doi:10.1016/j.visres.2008.09.029

future studies, the population of RGCs in these rats, the proportion of this population responsible for the retinotectal projection as well as their spatial distribution within the retina.

Using retrogradely transported tracers to label the entire RGC population and an automated methodology to count fluorogold (FG)-labelled RGCs (Danias et al., 2002; Salinas-Navarro et al., 2005) and to represent their detailed spatial distribution (Vidal-Sanz, Salinas-Navarro, et al., 2007; Villegas-Pérez et al., 2006), we report the numbers of rat RGCs that project along the optic nerve both in albino and pigmented adult rats. We have also determined the population of RGCs that project to the main target regions in the brain, the superior colliculi (SCi), and estimated the magnitude of the proportion of RGCs contributing to the retinotectal projection, providing direct evidence for the massive retinotectal projection in the retinofugal system of adult rats. We have also analysed the spatial distribution of RGCs within the retina using detailed isodensity maps, and found that there is a horizontally oriented region in the dorsal retina that contains the highest densities of RGCs, adopting the form of a visual streak (parts of this work have been presented in abstract form, Salinas-Navarro et al., 2005; Vidal-Sanz, Salinas-Navarro, et al., 2007; Villegas-Pérez et al., 2006).

2. Materials and methods

2.1. Animals and anesthetics

Experiments were performed on 33 albino Sprague–Dawley (SD) (33 female) and 33 pigmented Piebald Virol Glaxo (PVG) Brown Norway (5 male and 28 female) adult (180–200 g) rats, obtained from the breeding colony of the University of Murcia (Murcia, Spain). Rats were housed in temperature and light controlled rooms with a 12 h light/dark cycle and had food and water *ad libitum*. Light intensity within the cages ranged from 9 to 24 lux. Animal manipulations followed institutional guidelines, European Union regulations for the use of animals in research and the ARVO statement for the use of animals in ophthalmic and vision research. Moreover, adequate measures were taken to minimize pain or discomfort.

Surgical manipulations were carried out under general anesthesia induced with an intraperitoneal (i.p.) injection of a mixture of ketamine (70 mg/kg, Ketolar®, Parke-Davies, S.L., Barcelona, Spain) and xylazine (10 mg/kg, Rompún®, Bayer, S.A., Barcelona, Spain). During recovery from anaesthesia, rats were placed in their cages, and an ointment containing neomycin and prednisone (Oftalmolosa Cusí Prednisona-Neomicina®; Alcon S.A., Barcelona, Spain) was applied on the cornea to prevent corneal desiccation. Animals were sacrificed with an i.p. injection of an overdose of pentobarbital (Dolethal Vetoquinol®, Especialidades Veterinarias, S.A., Alcobendas, Madrid, Spain).

2.2. Retrograde labelling

2.2.1. Retrograde labelling from the optic nerve

To quantify the entire RGC population, FG was applied to the intraorbitally transected ON following previously described methods (Vidal-Sanz, Villegas-Pérez, Bray, & Aguayo, 1988; Villegas-Pérez et al., 1993) in 14 (female) SD and 3 (female) PVG rats. In brief, a small pledget of gelatine sponge soaked in saline containing 3% Fluorogold® (FG) (Fluorochrome Inc., Engelwood, CO, USA) and 10% dimethyl sulphoxide (DMSO) was applied to the ocular stump of the cut optic nerve, approximately 3 mm from the optic disc (Lafuente López-Herrera, et al., 2002; Villegas-Pérez et al., 1993), and the animals processed 3 days later.

2.2.2. Retrograde labelling from the superior colliculi

To identify the population of RGCs that project to the superior colliculi (SCi), their main target territory in the brain, we applied the fluorescent tracer FG to both SCi in 19 (female) SD and 30 (25 female; 5 male) PVG rats, following previously described methods (Vidal-Sanz et al., 1988) that are standard in our laboratory. In brief, after exposing the midbrain, a small pledget of gelatine sponge (Espongostan® Film, Ferrosan A/S, Denmark) soaked in saline containing 3% FG and 10% DMSO was applied over the entire surface of both SCi.

2.2.3. Double labeling of retinal ganglion cells

To further study the spatial distribution of RGCs, and to investigate whether the appearance of a RGC high-density region within the dorsal retina was the consequence of an artifact due to the labeling from the SCi, in 12 additional adult female SD rats we applied two retrogradely transported tracers with different fluorescence properties: FG and dextran tetramethylrhodamine (DTMR; 3000 MW; Molecular Probes, Inc. Eugene, OR, USA). FG was applied to both SCi and, 5 days later and 48 h prior to processing, small crystals of DMTR were applied to the ocular stump of the right ON, which had been intraorbitally sectioned approximately 2 mm from the eye, following previously described methods (Lafuente López-Herrera et al., 2002). DMTR diffuses passively through the axon towards the cell soma producing an intense cell labelling (WoldeMussie, Ruiz, Wijono, & Wheeler, 2001). In these animals, DMTR would label the entire retinofugal projection whereas FG would label only RGCs projecting to the SCi.

2.3. Tissue processing

Rats were deeply anesthetized, perfused transcardially through the ascending aorta first with saline and then with 4% paraformaldehyde in 0.1 M phosphate buffer (PB) (pH 7.4). For the present studies determining retinal orientation is crucial, thus special care was taken to maintain the orientation of each eye. Right after deep anesthesia and before fixation a suture was placed on the dorsal pole of each eye. Furthermore, the rectus muscle insertion into the dorsal part of the eye, as well as, the nasal caruncle were used as additional landmarks. Retinas from both eyes were dissected as flattened whole-mounts by making four radial cuts (the deepest one in the dorsal pole), post-fixed for an additional hour in the same fixative, rinsed in 0.1 M PB, mounted vitreal side up on subbed slides and covered with anti-fading mounting media containing 50% glycerol and 0.04% *p*-phenylenediamine in 0.1 M sodium carbonate buffer (pH 9.0).

2.4. Retinal analysis

Retinas were examined and photographed under a fluorescence microscope (Axioscop 2 Plus; Zeiss Mikroskopie, Jena, Germany) equipped with an ultraviolet (BP 365/12, LP 397) filter that allows the observation of the white-gold FG-fluorescence, and with a rhodamine (BP 450–490, LP 520) filter that allows the observation of the orange-red DTMR fluorescence. The microscope was also equipped with a digital high-resolution camera (ProgRes™ C10, Jenoptik, Jena, Germany), computer-driven motorized stage (ProScan™ H128 Series, Prior Scientific Instruments, Cambridge, UK), controlled by IPP (IPP 5.1 for Windows®; Media Cybernetics, Silver Spring, MD, USA) with a microscope controller module (Scope-Pro® 5.0 for Windows®; Media Cybernetics, Silver Spring, MD, USA), following standard procedures in our laboratory (Lafuente López-Herrera, et al., 2002; Vidal-Sanz, Lafuente, Mayor, Miralles de Imperial, & Villegas-Pérez, 2001). To make reconstructions of retinal whole-mounts, retinal multiframe acquisitions were acquired in a raster scan pattern using a x10 objective (Plan-Neofluar, 10×/0.30; Zeiss Mikroskopie, Jena, Germany). Single frames were focused manually prior to the capture of the digitized images. The scan area covers the entire retina and with a frame size of

0.627 mm^2/image, usually requires 154 images to be taken for each retina.

The images taken for each retina were saved as a set of 24-bit color image pictures and later, these images were combined into a single high-resolution composite image of the whole retina using IPP. Reconstructed images were further processed when required using Adobe Photoshop® CS 8.0.1 (Adobe Systems, Inc., San Jose, CA, USA).

2.5. Image processing

The individual FG-fluorescent images taken in each retina were processed by a specific cell counting subroutine that we developed to automate repetitive tasks. In brief, we used the IPP macro language to apply a sequence of filters and transformations to each image in order to clarify cell limits and separate individual cells for automatic cell counting. Initially, the images were converted to 8-bit grey scale images to discard the color information. Illumination aberrations caused by the microscope optics were removed by the flatten enhancement filter which evens out the background variations. This was followed by enhancement of the edges of the cells using the large spectral filter edge + command, which extracts positive edges (in this case fluorescently stained bright cells) from the dark background. A setting of 8% (kernel size 20 × 20) was sufficient to enhance the cell edges making detection simpler. Small artifacts and noise were removed by running three passes of the median enhancement filter (kernel size 3 × 3). Cell clusters were then separated by two passes of the watershed split morphological filter which erodes objects until they split and then dilates them until they do not touch. Finally, the cells in each image were counted using predetermined parameters to exclude objects that were larger than 300 μm^2 or smaller than 7 μm^2. These parameters correspond to the largest and smallest individual FG-labeled objects detected as RGCs. Finally, each count was exported to a spreadsheet (Microsoft® Office Excel 2003, Microsoft Corporation, Redmond, WA, USA) for statistical analysis.

2.6. Retina area measurement

Area of the retinas was measured on the high-resolution photomontage image of the whole retina with the IPP program calibrated off the stage movement. Retinal areas were measured over photomontages obtained from fixed retinas and thus, we ignore the degree of variation due to histological processing.

2.7. Isodensity maps

Using the cell counts obtained for each frame, we first constructed pseudo-colored density maps for each retina by estimating cell density in each of the 154 frames of the whole-mount and converting them manually to different colors using image editing software (Adobe® Photoshop®). This approach depicted an area of high density within the dorsal retina (Fig. 2C). The map was further refined by dividing each frame into four rectangular equally-sized regions and calculating the density in each of these regions again and converted them again to colors using the same software. This improved the resolution of the cell distribution throughout the retina (Fig. 2D). Finally, to demonstrate the distribution pattern of RGCs over the entire retina more graphically, cell densities were calculated and represented as filled contour plot graphs (Fig. 2E) using graphing software (SigmaPlot® 9.0 for Windows®, Systat Software, Inc., Richmond, CA, USA). Briefly, we developed a specific subroutine using IPP® macro language in which every frame was divided into 64 equally-sized rectangular areas of interest (AOI). In each AOI, the RGC number was obtained using the previously described cell counting subroutine and the cell density was calculated. RGC densities were later exported to a spreadsheet (Microsoft® Office Excel 2003, Microsoft Corporation, Redmond, WA) and finally, data was once more represented as filled contour plots (Fig. 2E) using a graphing software (Sigmaplot®). Cell density calculating errors due to frames not fully occupied by retinal tissue on the whole retina contour were minimized by the high number of AOI with a relatively small size in each frame and by the near absence of RGCs in the retinal periphery.

2.8. Method validation

To validate the automatic counting method, four different experienced investigators counted in a blind masked fashion FG-labelled RGCs in 40 frames randomly selected from both eyes and representing different density regions of 4 normal rat retinas. These 40 frames were also counted automatically and the results were compared to those obtained manually (Fig. 1).

The criteria used for identifying and counting manually a FG-labelled RGC have been described in detail elsewhere (Vidal-Sanz et al., 2001; Lafuente et al., 2002, Lafuente López-Herrera, et al., 2002). In brief, FG-labelled RGCs had the typical punctuate and diffuse gold fluorescence delineating their somas and occasionally the initial segments of their primary dendrites (Fig. 2). A labeled RGC was counted if the whole cell was included within the frame or the nucleus of the cell was visible within the micrograph.

2.9. Statistics

Statistical analysis of the differences between groups of retinas or groups of animals was done using non-parametric ANOVA tests using Statistix® V1.0 for Windows® 95 software: the Kruskal–Wallis test was used to compare more than two groups and the Mann–Whitney test was used when comparing two groups only. To compare values from both retinas of different rats we used the paired *t*-test. Cell counts obtained by the automated method were compared with those obtained with the manual method using the Pearson correlation test (SigmaStat® for Windows™

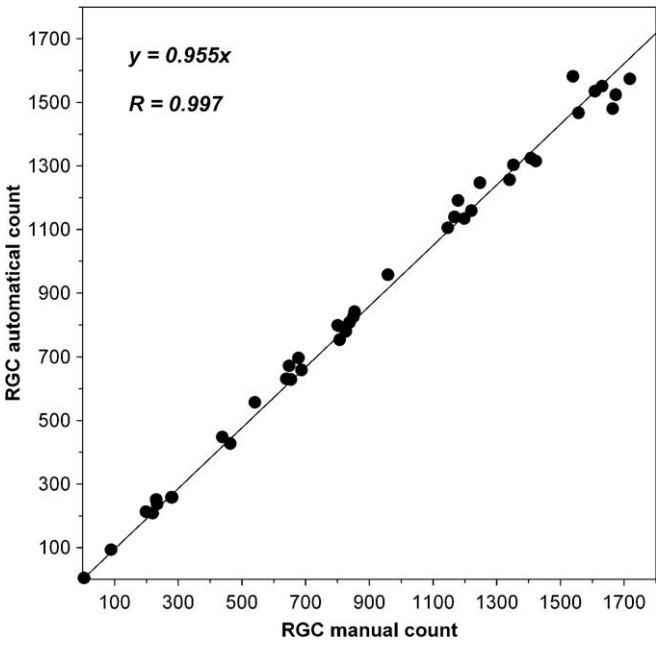

Fig. 1. Validation of automated RGC counting. Correlation of the numbers of RGCs counted manually versus automated methods in 40 frames randomly selected with different RGC densities. The black line is the line of best fit for the data, for which the equation and correlation coefficient are displayed on the graph.

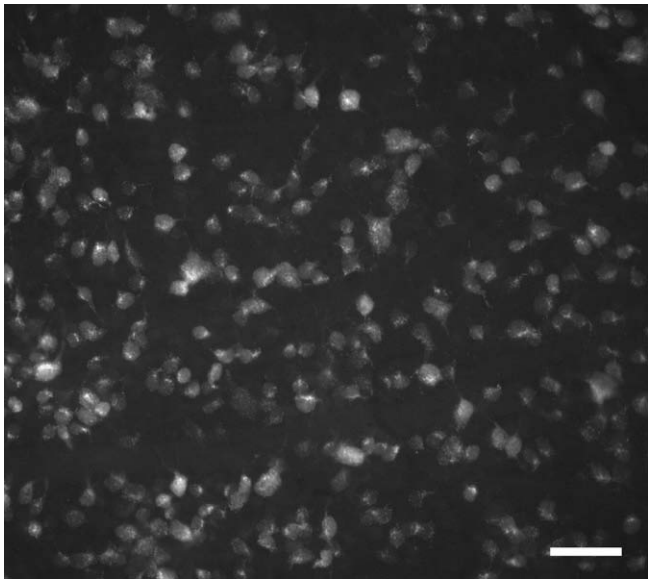

Fig. 2. Fluorescence micrograph from a representative flat-mounted retina showing at high magnification retinal ganglion cells retrogradely labelled with FG applied to both SCi for seven days prior to processing. The micrograph was taken on the periphery of the retina. Scale bar, 50 μm.

Version 3.11; Systat Software, Inc., Richmond, CA, USA). Differences were considered significant when $P < 0.05$.

3. Results and discussion

In this study, we have examined the total numbers and spatial distribution of RGCs in adult albino (SD) and pigmented (PVG) rats. As revealed by retrograde axoplasmic transport of FG, there are approximately 82,818 and 89,241 RGCs, in the albino and pigmented rat, respectively. The numbers of RGCs retrogradely labeled from both SCi in SD and PVG rats were slightly smaller (1.6% and 2.2%, respectively) but comparable to those retrogradely labeled from the optic nerves showing, as previously suggested (Lund, 1965; Perry, 1981), that most RGCs project to the SCi, and providing additional evidence for the massive retinotectal projection in the retinofugal system of adult rats. There were significant differences between the total numbers of RGCs in the albino and pigmented rats, which probably reflect a strain difference. The spatial distribution of RGCs within the retina demonstrated a horizontally oriented area of highest density located in the dorsal retina, resembling a visual streak.

3.1. Validation of cell counts

The accuracy of automatic counting was evaluated by comparing manual counts obtained by different expert investigators. Thus, in 40 randomly selected frames from right and left retinas, FG-labelled RGCs were counted manually by four different investigators blinded to the conditions compared. These results were plotted against the counts obtained automatically with the analysis program. There was a strong correlation between both methods (Pearson correlation test, $R = 0.997$; $P < 0.0001$) (Fig. 1).

Previous work in our laboratory requiring quantitative estimates of the retinal ganglion cell (RGC) population has consisted of manual counts of identified retrogradely labelled RGCs over printed photographs of standard regions of the retina, and the sampled area was only a small portion of the retina. Although manual cell counting may be accurate in the hands of an expert researcher (Vidal-Sanz et al., 2001), it is an often tedious, time-consuming and biased method. The need for obtaining a reliable, rapid and objective counting procedure appears of importance in experiments aimed at investigating neuronal survival on injury-induced neuronal death or as a baseline in a range of developmental studies. Thus, even though there is no perfect method for counting cells (Guillery, 2002), the present methodology is unbiased because it is performed by the software analysis program. Moreover, based on our cell count validation results it is also accurate. In addition, our results shown below indicate that it is a reliable and reproducible method to count RGCs, and indeed the total counts of RGCs were quite reproducible from retina to retina in our groups of SD or PVG rat (Tables 1–4).

However, this method to quantify the RGC population with the application of FG is of limited use in experimental designs in which the tracer cannot be applied to the retinofugal system (e.g., in experiments that involve a previous lesion of the ON) and relies

Table 1
Number of ganglion cells retrogradely labeled from the optic nerve (SD rats).

Animal #	Right retina			Left retina		
	Cells	Area (mm^2)	Mean cell density (Cells/mm^2)	Cells	Area (mm^2)	Mean cell density (Cells/mm^2)
1	82896	49.9	1660	78994	50.8	1554
2	79498	51.0	1558	77408	52.0	1489
3	87575	48.6	1803	82667	49.5	1671
4	80249	48.8	1646	84756	50.7	1672
5	88101	55.2	1597	82223	47.7	1723
6	82380	49.0	1683	82092	50.6	1622
7	78127	44.2	1769	80812	48.9	1652
8	87643	47.9	1831	–	–	–
9	83871	43.9	1911	77648	48.4	1603
10	84605	51.7	1636	89613	51.0	1758
11	85510	47.4	1804	90749	51.6	1760
12	80299	49.2	1633	88766	49.8	1781
13	79747	46.3	1722	79696	49.0	1627
14	77257	49.4	1565	82915	49.8	1665
Mean	82697[b]	48.8	1701	82949[b]	50.0	1660
SD	3634	2.9	108	4409	1.3	84
n	14	14	14	13	13	13
Mean[a]	82818	49.3	1681			
SD[a]	3949	2.3	97			
n	27	27	27			

[a] Data from both retinas.
[b] Not significantly different (Paired *t*-test, $P = 0.654$).

Table 2
Number of ganglion cells retrogradely labeled from the optic nerve (PVG rats).

Animal #	Right retina			Left retina		
	Cells	Area (mm^2)	Mean cell density (Cells/mm^2)	Cells	Area (mm^2)	Mean cell density (Cells/mm^2)
1	89894	58.08	1548	92844	61.87	1501
2	93012	60.26	1544	89673	60.14	1491
3	85435	57.4	1488	84588	59.12	1431
Mean	89447[b]	58.6	1527	89035[b]	60.4	1474
SD	3808	1.5	34	4165	1.4	38
n	3	3	3	3	3	3
Mean[a]	89241	59.5	1501			
SD[a]	3576	1.6	43			
n	6	6	6			

[a] Data from both retinas.
[b] Not significantly different (Paired *t*-test, $P = 0.8427$).

Table 3
Number of ganglion cells retrogradely labeled from the superior colliculi (SD rats).

Animal #	Right retina			Left retina		
	Cells	Area (mm^2)	Mean cell density (Cells/mm^2)	Cells	Area (mm^2)	Mean cell density (Cells/mm^2)
1	80324	53.2	1509	72595	55.7	1304
2	77501	53.2	1456	82633	56.0	1475
3	83360	54.9	1520	81688	54.3	1504
4	87570	57.0	1536	86031	57.0	1509
5	76842	51.2	1500	74551	48.0	1553
6	72454	45.6	1589	72802	48.6	1497
7	83268	50.1	1661	80798	48.7	1660
8	80207	48.6	1650	79695	50.7	1571
9	81705	46.5	1756	82530	50.8	1626
10	83713	48.4	1731	82357	47.4	1737
11	84744	52.7	1609	81144	52.0	1561
12	90166	46.8	1927	89465	49.9	1792
13	86771	50.5	1717	85735	51.2	1674
14	85510	50.0	1712	–	–	–
15	77872	48.2	1617	78922	52.6	1500
16	79794	50.1	1593	78423	48.5	1617
17	81794	55.7	1469	77978	53.2	1465
18	84586	50.1	1688	84528	51.5	1641
19	82806	53.7	1543	82127	54.5	1507
Mean	82157[b]	50.9	1620	80778[b]	51.7	1566
SD	4214	3.2	118	4478	2.9	114
n	19	19	19	18	18	18
Mean[a]	81486	51.3	1594			
SD[a]	4340	3.1	118			
n	37	37	37			

[a] Data from both retinas.
[b] Not significantly different (Paired *t*-test, $P = 0.0655$).

on an efficient method to apply the tracer (Vidal-Sanz et al., 2001) and on the competence of the retrograde axonal transport (Lafuente López-Herrera, et al., 2002). Moreover, in the present studies we could not analyze the size of the cell somas due to the transformations imposed to the FG-labeled RGCs in the analysis process.

3.2. Population of RGCs in SD and PVG rats

3.2.1. General appearance

Application of tracer to the intraocular aspect of the ON or to both SCi resulted in retinae that showed RGCs typically labeled with bright punctate and diffuse FG-fluorescence delineating their soma and occasionally the initial segment of their primary dendrites (Fig. 2) (Lafuente López-Herrera, et al., 2002; Peinado-Ramón et al., 1996; Sellés-Navarro et al., 1996; Vidal-Sanz et al., 2001). These cells were distributed throughout the RGC layer of the retina in a regular fashion with clusters containing higher cell densities in the central regions of the retina (Fig. 3A). When focusing on the inner nuclear layer of the retina, small numbers of displaced RGCs were observed, but these (so called Dogiel's cells) have not been taken into account for the present study.

3.2.2. RGCs retrogradely labeled from the ON

In the group of 14 SD rats in which their retinas were labeled with FG applied to the intraorbital aspect of the ON for 3 days, the mean number of FG-labeled RGCs in the 27 analyzed retinas was 82,818 ± 3,949 (mean ± SD) (Table 1). There were no significant differences between the numbers of FG-labeled RGCs obtained in the right retinas when compared to their fellow contralateral left retinas (Paired *t*-test, $P = 0.654$; $n = 13$) (Table 1). In the group of 3 PVG rats in which their retinas were labeled with FG applied to the intraorbital aspect of the ON for 3 days, the mean number of FG-labeled RGCs was 89,241 ± 3,576 ($n = 6$; mean ± SD) (Table 2). There were no significant differences between the numbers of FG-labelled RGCs obtained in the right retinas when compared to their fellow contralateral left retinas (Paired *t*-test, $P = 0.8427$; $n = 3$) (Table 2).

Table 4
Number of ganglion cells retrogradely labeled from the superior colliculi (PVG rats).

Animal #	Right retina			Left retina		
	Cells	Area (mm^2)	Mean cell density (Cells/mm^2)	Cells	Area (mm^2)	Mean cell density (Cells/mm^2)
1	84121	48.1	1747	82232	50.0	1646
2	87235	48.5	1799	85300	55.3	1544
3	87920	49.4	1779	86889	49.1	1770
4	82599	48.8	1694	80348	52.8	1522
5	87623	53.9	1626	84128	52.8	1594
6	82186	46.8	1756	82920	50.6	1640
7	87732	54.1	1623	90951	56.3	1617
8	86469	54.6	1583	89508	54.9	1630
9	88725	52.2	1701	88384	55.4	1597
10	86812	51.5	1686	88927	56.7	1568
11	90797	55.9	1625	90523	56.2	1612
12	92557	58.9	1571	93876	59.2	1587
13	92985	59.4	1566	94101	60.7	1551
14	89491	61.5	1456	88438	58.3	1517
15	90499	59.5	1520	89596	61.4	1460
16	84475	53.3	1585	86891	57.3	1518
17	89482	56.1	1594	85657	52.7	1625
18	90772	58.0	1565	83342	57.9	1439
19	87495	54.7	1599	89399	57.6	1552
20	90556	57.4	1578	89001	58.0	1534
21	87924	54.8	1605	87038	53.5	1627
22	89494	53.9	1662	90498	55.2	1639
23	80050	55.1	1454	-	-	-
24	88982	55.4	1608	87762	52.8	1662
25	88187	58.4	1509	87989	54.8	1605
26[b]	85940	48.3	1780	86531	49.8	1739
27[b]	84519	48.6	1741	85424	49.4	1731
28[b]	84742	49.5	1713	82491	51.3	1609
29[b]	84582	49.0	1727	84763	50.5	1678
30[b]	84001	49.0	1715	84643	47.4	1788
Mean	87298[c]	53.5	1639	87157[c]	54.4	1607
SD	3110	4.1	95	3343	3.7	84
n	30	30	30	29	29	29
Mean[a]	87229	53.9	1623			
SD[a]	3199	3.9	90			
n	59	59	59			

[a] Data from both retinas.
[b] Male rats.
[c] Not significantly different (Paired *t*-test, $P = 0.3583$).

3.2.3. RGCs retrogradely labeled from the SCi

The numbers of FG-labeled RGCs in the SD rat retinas 7 days after FG application to the SCi were 81,486 ± 4,340 ($n = 37$; mean ± SD) (Table 3). There were no significant differences between the numbers of FG-labeled RGCs obtained in the right retinas when compared to their fellow contralateral left retinas (Paired *t*-test, $P = 0.0655$; $n = 18$) (Table 3). In PVG rats, the total numbers of FG-labeled RGCs from the SCi were 87,229 ± 3,199 ($n = 59$; mean ± SD) (Table 4). There were no significant differences between the numbers of FG-labeled RGCs obtained in the right retinas when compared to their fellow contralateral left retinas (Paired *t*-test, $P = 0.3583$; $n = 29$) (Table 4). Thus, the two retinas of an individual animal have comparable numbers of RGCs).

The overall mean number of FG-labelled RGCs obtained when FG was applied intraorbitally was slightly greater than that obtained when FG was applied to both SCi. In SD rats, approximately 1.6% of the population of RGCs that were labeled from the ON did not project to the SCi, a difference that was not statistically significant (Tables 1 and 3; Mann Whitney test, $P = 0.3588$). Similarly, for the groups of PVG rats, approximately 2.2% of the population of RGCs that were labeled from the ON did not project to the SCi, a difference that was not statistically significant (Tables 2 and 4; Mann–Whitney test, $P = 0.1438$). This finding is in agreement with previous studies and provides additional evidence documenting that there is a massive projection from the retina towards the tecta (Linden & Perry, 1983; Lund, 1965, 1969; Lund, Land, & Boles, 1980). Other studies have also indicated that most axons project to the tectum and that the retinogeniculate projection is formed out of branches from approximately 35% of the retinotectal axons (Dreher et al., 1985; Martin, 1986).

The overall numbers of FG-labelled RGCs obtained in the PVG rats were greater than those obtained in SD rats, either when FG was applied to both SCi for 7 days (Tables 3 and 4; Mann–Whitney test, $P = 0.0000$) or to the intraorbital aspect of the optic nerve for 3 days (Tables 1 and 2; Mann–Whitney test, $P = 0.0035$), and this may reflect genetic differences between albino and pigmented rats (Fukuda, Sugimoto, & Shirokawa, 1982; Williams, Strom, Rice, & Goldowitz, 1996) or developmental differences in the early outgrowth of optic axons (Bunt, Lund, & Land, 1983) or the consequences of an abnormal laterality of distribution of optic axons in albinos (Fleming, Benca, & Behan, 2006; Lund, 1965). Behavioural studies involving visual acuity tests have also reported differences between albino and pigmented rats, the latter showing an enhanced visual acuity when compared to albino (Prusky, Harker, Douglas, & Whishaw, 2002).

The present studies were not designed to investigate the numbers of RGCs that project ipsi- or contralaterally to the SCi, but rather to quantify the population of RGCs contributing to the retinotectal projection. In our experience, FG application to the surface of one midbrain may also result in spurious labeling of the contralateral midbrain, because FG is a highly soluble dye. Other studies have indicated that the total number of RGCs that project ipsilater-

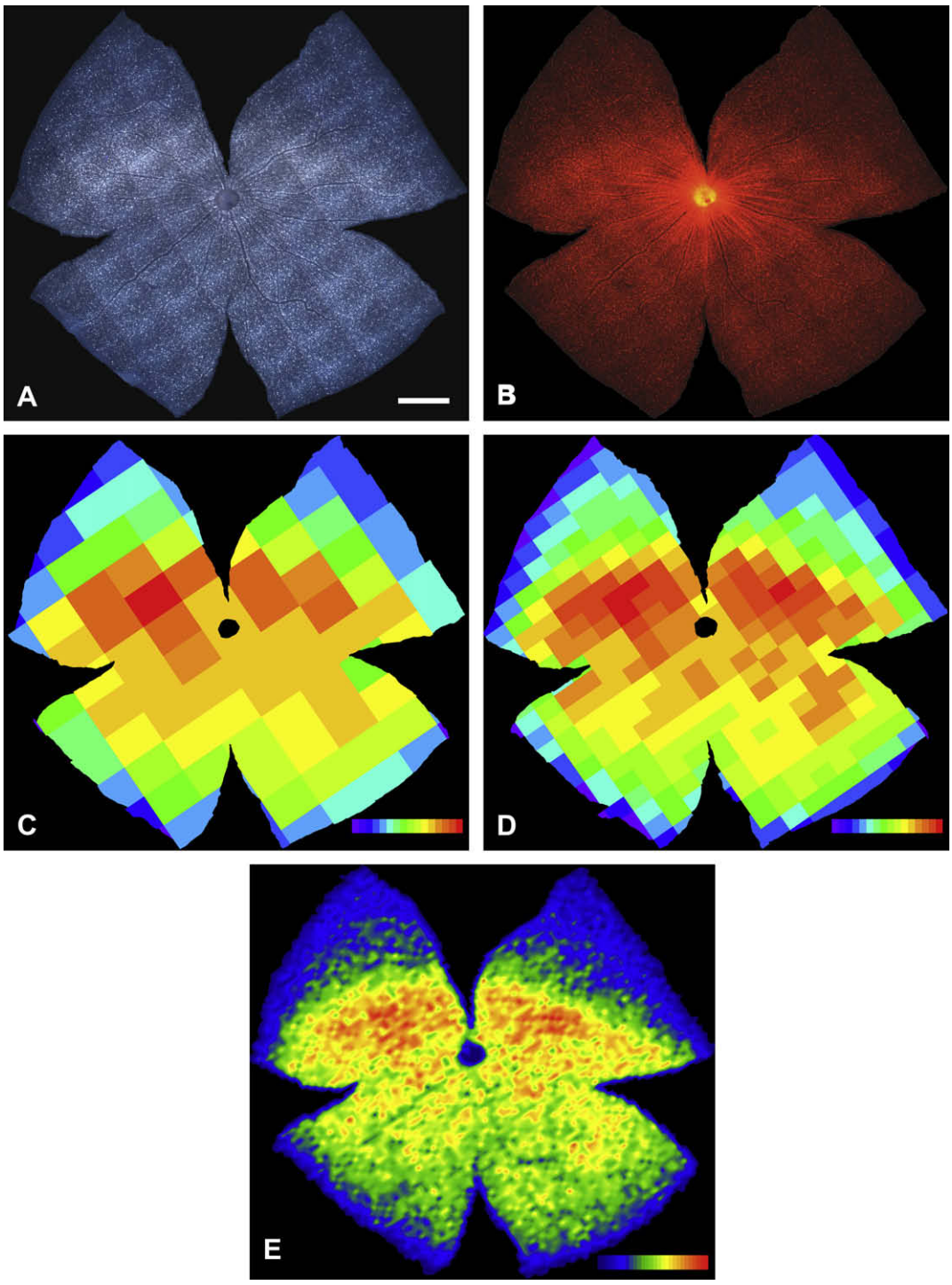

Fig. 3. Whole-mount of a representive SD right rat retina showing RGCs, double labelled with FG (A) applied to both SCi for 7 days and with DTMR (B) applied to the ocular stump of the intraorbitally transected ON 5 days later, distributed with a higher density along a naso-temporal streak in the dorsal retina. Color-coded density maps (C–E). Density maps generated by assigning to each individual frame (C) or each one of the four subdivisions from each individual frame (D) a color code according to its RGC density value within a 16-step color scale ranges from 0 (violet) to 3,000 or higher RGCs/mm^2 (red). Isodensity map (E) is represented as a filled contour plot generated by assigning to each one of the 64 subdivisions of each individual frame a color code according to its RGCs density value within a 28-step color scale range from 0 (dark blue) to 3500 or higher RGCs/mm^2 (red). For all retinas the dorsal pole is orientated at the 12 o'clock orientation. This retina has 76,390 FG-labeled RGCs. Scale bar, 1 mm.

ally in a range of rodents (e.g., Syriam hamsters, Métin, Irons, & Frost, 1995; adult rats, Cusick & Lund, 1982; Lund et al., 1980) has been estimated to be of approximately 2.6–5% of the RGC population.

The numbers of RGCs obtained in our experiments are comparable to other studies that have investigated the numbers of RGCs in albino or pigmented rats. For instance, in Wistar rats, Levkovitch-Verbin et al., 2003 have estimated a total number of axons in the ON behind the eye to be 85,511. Using stereologic protocols Freeman and Grosskreutz (2000) estimated a total number of RGCs in the adult Wistar rat of 74,104 and Levkovitch-Verbin et al., 2003 found that the total number of RGCs was 87,809 per eye. Using 4Di-10ASP applied to both SC and sampling regions of the retina, Fischer and colleagues (2000) estimated the total number of RGCs in SD rats to be 77,400.

Our numbers however, are somewhat smaller than those reported by Siu and colleagues (2002) who estimated from sampling areas of SD rat retinas that the total number of RGCs, using FG as a retrograde tracer applied to both SCi, is of approximately 98,725. Ko and colleagues (2001) found in Wistar rats a total of 119,988 RGCs. Using a similar approach Danias and colleagues (2006) found in Wistar and Brown Norway rats a total number of RGCs of 112,128 and 72,707, respectively. These differences may be explained by areal differences in RGC density across the retinal area, the number of areas examined, the different strains employed for the study, the tracers employed and mode of application, or on the methods employed to estimate the total RGC population.

3.3. Retinal area and densities of RGCs in SD and PVG rats

In the SD groups of rats that were labeled with FG applied to both SCi, the areas varied between 45.6 and 57 mm^2 with a mean value of 51.3 ± 3.1 (n = 37; mean ± SD). In these retinas, the local densities of FG-labeled RGCs varied between 1304 and 1927 with a mean of 1594 ± 118 (n = 37; mean ± SD) (Table 1). In the SD group of rats that were labeled with FG applied to both ONs, the areas varied between 44.2 and 55.2 mm^2 with a mean value of 49.3 ± 2.3 (n = 27; mean ± SD). In these retinas, the densities varied between 1489 and 1911 with a mean of 1681 ± 97 (n = 27; mean ± SD). (Table 3).

In the PVG group of rats that were labeled with FG applied to both SCi, the areas varied between 46.8 and 61.5 mm^2 with a mean value of 53.9 ± 3.9 (n = 59; mean ± SD) (Table 2). In these retinas, the local densities varied between 1439 and 1799 with a mean of 1623 ± 90 (n = 59; mean ± SD) (Table 2). In the PVG group of rats that were labeled with FG applied to both ONs, the areas varied between 57.4 and 61.9 mm^2 with a mean value of 59.5 ± 1.6 (n = 6; mean ± SD) (Table 4). In these retinas, the local densities varied between 1431 and 1548 with a mean of 1501 ± 43 (n = 6; mean ± SD) (Table 4).

Overall, our values obtained in the groups of SD or PVG rats for the densities of RGCs are within the range reported for albino or pigmented rats in previous studies from other independent laboratories (Ahmed, Hegazy, Chaudhary, & Sharma, 2001; Blair et al., 2005; Klöcker, Zerfowski, Gellrich, & Bähr, 2001; Park, Cozier, Ong, & Caprioli, 2001; Schuettauf, Naskar, Vorwerk, Zurakowski, & Dreyer, 2000; Swanson, Schlieve, Lieven, & Levin, 2005; Thanos, Mey, & Wild, 1993; WoldeMussie et al., 2001).

Nevertheless, when central regions of the retina are sampled, the densities of FG-labelled RGCs tend to be significantly higher. This is reflected in previous studies from this (Lafuente, López-Herrera, et al., 2002; Peinado-Ramón et al., 1996; Sellés-Navarro et al., 1996; Vidal-Sanz et al., 1988, 2001; Villegas-Pérez et al., 1988) and other laboratories (Bakalash, Kipnis, Yoles, & Schwartz, 2002; Mo et al., 2002; Nakazawa, Tamai, & Mori, 2002; Pavlidis, Fischer, & Thanos, 2000) and may be explained by the different distribution of RGC throughout the retina, with highest densities in central regions (Fukuda, 1977; McCall et al., 1987; Perry, 1981; Schober & Gruschka, 1977; see below).

3.4. Retinal distribution of RGCs

Microscopic examination of the retinas revealed that the FG-labeled RGCs were not uniformly distributed throughout the retina. There were higher densities of FG-labeled RGCs in the central regions of the retina when compared to the periphery (see Fig. 3A). Although there was certain variability in the location of highest RGC density areas within each of the retinas, there was a tendency for higher densities to be located in the dorsal retina, within the central region, forming a horizontally oriented area of high density that extended along the naso-temporal axis, approximately 1 mm dorsal to the optic disc.

Table 5
Number of ganglion cells retrogradely labeled from the superior colliculi (SD rats).

Animal #	Right retina		
	Cells	Area (mm^2)	Mean cell density (Cells/mm^2)
1	75644	51.0	1482
2	78311	53.6	1461
3	70766	55.6	1273
4	76690	51.8	1481
5	76390	45.2	1689
6	75731	55.0	1376
7	84028	51.0	1647
8	85231	53.1	1605
9	83651	51.2	1634
10	80973	51.6	1571
11	80879	55.7	1452
12	87705	55.7	1574
Mean	79667	52.5	1520
SD	4917	3.0	122
n	12	12	12

To discard the possibility that this high-density region in the dorsal retina was the result of an artifact due to retrograde labeling from the SCi, in 12 additional SD rats the RGC population of the right retina was double labeled with FG applied to both SCi for 7 days and with DTMR applied to the ocular stump of the intraorbitally transected right ON for two days. When these retinas were examined under the fluorescence microscope with different fluorescence filters (ultraviolet or rhodamine) it was found that almost every FG-labeled RGC was also double labeled with RITC but not vice versa; detailed quantification of these proportions was not undertaken. These double labeled retinas also showed the characteristic high-density region in the dorsal retina when observed under both fluorescent filters, indicating that the spatial distribution was not the result of a labeling artifact. A representative example of this observation is illustrated in Fig. 3A and B. The total numbers of FG-labeled RGCs in these right retinas (79,667 ± 4,917; mean ± SD; n = 12; Table 5) were comparable to those found in the group of animals in which RGCs were labeled from the SCi (Mann–Whitney test, P = 0.2498). Similarly the mean areas of these retinas were comparable to those found in such previous group of SD rats (Table 5).

To analyze in more detail this high-density region that adopted the form of a visual streak, we constructed color-coded density maps for these 12 retinas (Fig. 3C). The color-coded density maps confirmed our qualitative impression of a region with the highest density located in the dorsal retina. A further analysis of the high-density region involved the construction of finer density maps, in which individual frame was subdivided by 4 and color-coded in a scale of 16 different steps (each of 187.5) ranging from 0 to 3000 FG-labelled RGCs/mm^2 (an illustrative example of these finer density maps is shown in Fig. 3D). These maps showed evidence that there was a high-density region located approximately along the naso-temporal axis on the dorsal retina forming a visual streak. From this high-density region, RGC densities fall off rapidly from this area towards the dorsal and ventral retina, but it does so more pronouncedly on the dorsal retina, with a clear gradient toward the periphery (Dreher et al., 1985; Fukuda, 1977; McCall et al., 1987; Perry, 1981; Schober & Gruschka, 1977).

This region of high RGC density was further documented using a filled contour plot graph to construct colored isodensity maps in a scale of 28 different steps (each of 125) ranging from 0 to 3500, and in which every frame was divided into 64 equally-sized rectangular areas, with comparable results in the 74 retinas analyzed (33 retrogradely labeled from the ON and 41 from the SCi). Demonstrative examples of these findings are illustrated in Figs. 3E, 4 and 5. The mean for the highest individual densities were 3579 ± 169

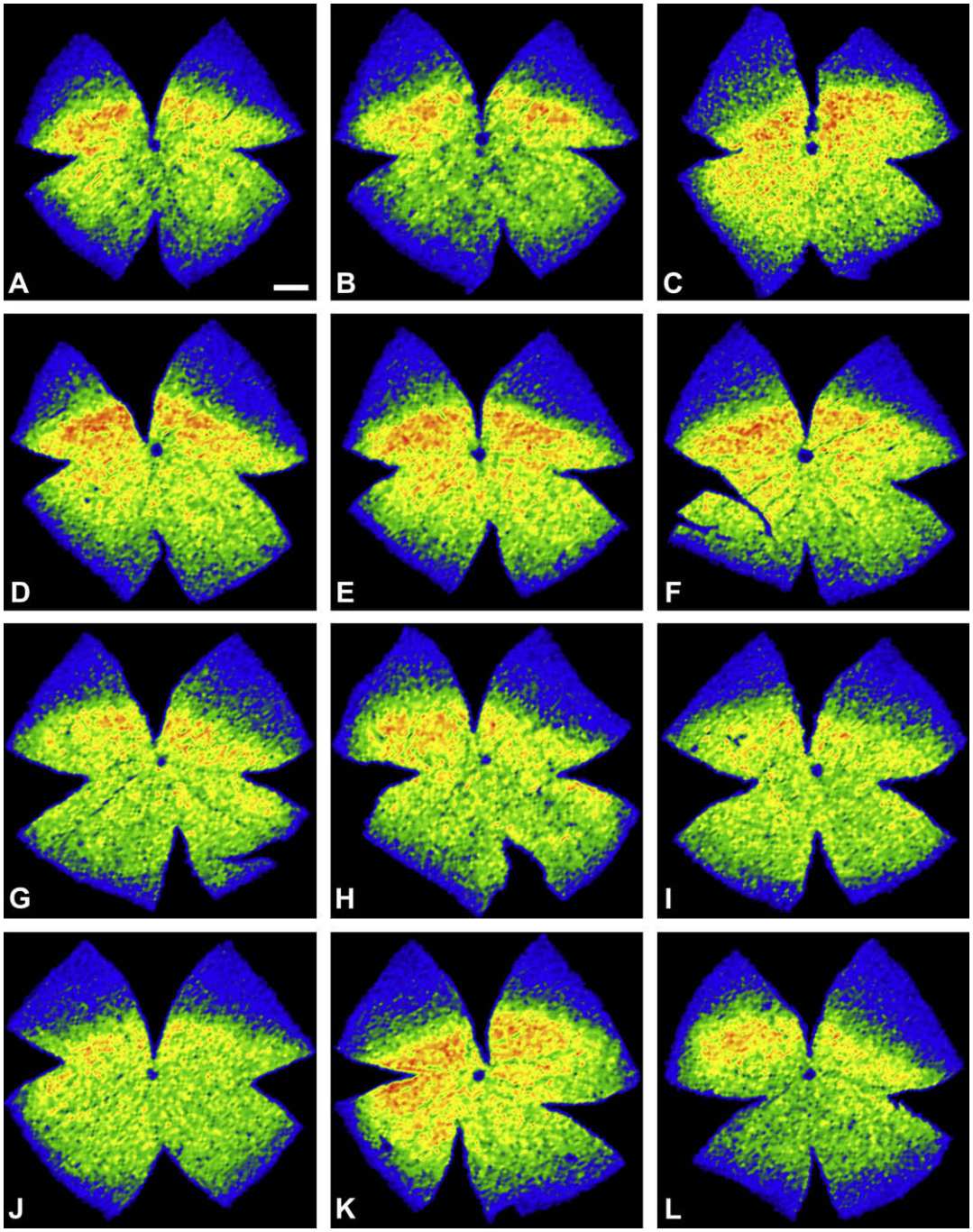

Fig. 4. Isodensity maps represented as a filled contour plot for six representative right SD rat retinas (A–F) and six representative PVG rat retinas (G and H are left retinas and I–L are right retinas). RGCs, were retrogradely labelled with FG applied to both SCi for 7 days. Isodensity maps are represented as a filled contour plot generated by assigning to each one of the 64 subdivisions of each individual frame a color code according to its RGCs density value within a 28-step color scale range from 0 (dark blue) to 3500 or higher RGCs/mm^2 (red). The high RGC density areas are within the dorsal retina along the naso-temporal axis. For all retinas the dorsal pole is orientated at the 12 o'clock orientation. Scale bar, 1 mm.

(n = 12; mean ± SD) or 3,334 ± 167 (n = 29; mean ± SD) for SD or PVG rat retinas, respectively, when FG was applied to both SCi and 3809 ± 249 (n = 27; mean ± SD) or 3504 ± 245 (n = 6; mean ± SD) for the SD or PVG rat retinas, respectively, when FG was applied to the ON.

The distribution of this high-density region in the dorsal retina resembles a visual streak located on the area of the retina that looks out to the horizon (Stone, 1983). Such regional specialization of the RGC distribution in the retina was previously observed and suggested in the hamster (Métin et al., 1995) and in the rat (Jeffery, 1985; Reese & Cowey, 1986) and has been shown by this Laboratory in the pigmented non-dystrophic RCS rat (Marco-Gomariz, Hurtado-Montalbán, Vidal-Sanz, Lund, & Villegas-Pérez, 2006). This finding may be at odds with a previous study in Wistar rats (Danias et al., 2002; Reese, 2002), but in our analysis we did not find clear evidence for the visual streak until the high-resolution density maps were constructed (Figs. 3C–E, 4 and 5A and B). Furthermore, even though our detailed filled contour plot graph based isodensity maps indicate the presence in the dorsal retina of an elongated region of elevated RGC density horizontally oriented along the naso-temporal axis, the highest density clusters of RGCs tended to localize on the dorsal temporal quadrant in most

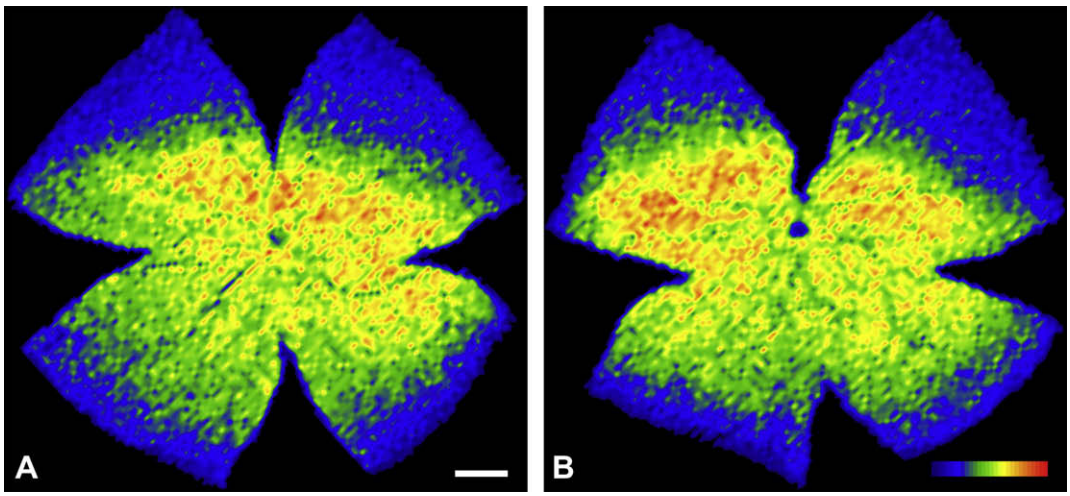

Fig. 5. Isodensity maps represented as a filled contour plot for both left (A) and right (B) retinas, from a representative SD rat labelled with FG applied to the ocular stump of the intraorbitally transected ON for 3 days, showing the typical high-density distribution along a naso-temporal streak in the dorsal retina. Maps were generated by assigning to each one of the 64 subdivisions of each individual frame a color code according to its RGCs density value within a 28-step color scale range from 0 (dark blue) to 3500 or higher RGCs/mm^2 (red). For all retinas the dorsal pole is orientated at the 12 o'clock orientation. Scale bar, 1 mm.

retinas, and this is in agreement with previous studies (Dreher et al., 1985; Fukuda, 1977; McCall et al., 1987; Métin et al., 1995; Schober & Gruschka, 1977).

4. Summary

In SD and PVG strain of rats, the population of RGCs labeled with FG from the ON or the SCi, may be counted automatically with a level of confidence that is comparable to that found when RGCs are counted manually. Our results indicate that only a small percentage of the RGC population does not contribute to the retinotectal projection. In addition we also provide evidence for the distribution of rat retinal ganglion cells adopting a form of regional specialization that resembles a horizontal visual streak rather than an area centralis. Overall, the consistency and similarity of the results obtained in the present studies speak for the presently used method as an unbiased, reliable, reproducible and accurate way to assess the RGC population in adult rats, with a level of accuracy hardly attained with other methods. Morever, the detailed isodensity maps constructed out of these counts provide a unique graphic system to assess regional RGC distribution in normal circumstances and after injury (Garcia-Ayuso et al., 2008; Marco-Gomariz et al., 2006) and neuroprotection in several experimental models (Salinas-Navarro et al., 2006; Schnebelen et al., 2007, 2008; Vidal-Sanz et al., De la Villa, 2007).

Acknowledgments

The authors thank the technical contribution of M.E. Aguilera, J.M. Bernal and I. Cánovas.

Support: This work was supported by research grants from the Regional Government of Murcia CARM BIO2005/016469; Fundación Séneca 02989/PI/05, 05703/PI/07, 04446/GERM/07; Spanish Ministry of Education and Science SAF-2005-04812; and Spanish Ministry of Health ISCIII: FIS PIO06/0780 and RD07/0062/0001; and an unrestricted grant from Allergan Inc.

References

Ahmed, F. A., Hegazy, K., Chaudhary, P., & Sharma, S. C. (2001). Neuroprotective effect of alpha(2) agonist (brimonidine) on adult rat retinal ganglion cells after increased intraocular pressure. *Brain Research, 21*, 133–139.

Avilés-Trigueros, M., Mayor-Torroglosa, S., García-Avilés, A., Lafuente, M. P., Rodríguez, M. E., Miralles de Imperial, J., et al. (2003). Transient ischemia of the retina results in massive degeneration of the retinotectal projection: long-term neuroprotection with brimonidine. *Experimental Neurology, 184*, 767–777.

Avilés-Trigueros, M., Sauvé, Y., Lund, R. D., & Vidal-Sanz, M. (2000). Selective innervation of retinorecipient brainstem nuclei by retinal ganglion cell axons regenerating through peripheral nerve grafts in adult rats. *Journal of Neuroscience, 20*, 361–374.

Bakalash, S., Kipnis, J., Yoles, E., & Schwartz, M. (2002). Resistance of retinal ganglion cells to an increase in intraocular pressure is immune-dependent. *Investigative Opthalmology and Visual Science, 43*, 2648–2653.

Blair, M., Pease, M. E., Hammond, J., Valenta, D., Kielczewski, J., Levkovitch-Verbin, H., et al. (2005). Effect of glatiramer acetate on primary and secondary degeneration of retinal ganglion cells in the rat. *Investigative Ophthalmology and Visual Science, 46*, 884–890.

Bunt, S. M., Lund, R. D., & Land, P. W. (1983). Prenatal development of the optic projection in albino and hooded rats. *Brain Research, 282*, 149–168.

Cusick, C. G., & Lund, R. D. (1982). Modification of visual callosal projections in rats. *Journal of Comparative Neurology, 212*, 385–398.

Danias, J., Shen, F., Goldblum, D., Chen, B., Ramos-Esteban, J., Podos, S. M., et al. (2002). Cytoarchitecture of the retinal ganglion cells in the rat. *Investigative Opthalmology and Visual Science, 43*, 587–594.

Danias, J., Shen, F., Kavalarakis, M., Chen, B., Goldblum, D., Lee, K., et al. (2006). Characterization of retinal damage in the episcleral vein cauterization rat glaucoma model. *Experimental Eye Research, 82*, 219–228.

Dreher, B., Sefton, A. J., Ni, S. Y., & Nisbett, G. (1985). The morphology, number, distribution and central projections of class I retinal ganglion cells in albino and hooded rats. *Brain Behavioural Evolution, 26*, 10–48.

Fischer, D., Pavlidis, M., & Thanos, S. (2000). Cataractogenic lens injury prevents traumatic ganglion cell death and promotes axonal regeneration both in vivo and in culture. *Investigative Ophthalmology and Visual Science, 41*, 3943–3954.

Fleming, M. D., Benca, R. M., & Behan, M. (2006). Retinal projections to the subcortical visual system in congenic albino and pigmented rats. *Neuroscience, 143*, 895–904.

Freeman, E. E., & Grosskreutz, C. L. (2000). The effects of FK506 on retinal ganglion cells after optic nerve crush. *Investigative Ophthalmology and Visual Science, 41*, 1111–1115.

Fukuda, Y. (1977). A three-group classification of rat retinal ganglion cells: Histological and physiological studies. *Brain Research, 119*, 327–334.

Fukuda, Y., Sugimoto, T., & Shirokawa, T. (1982). Strain differences in quantitative analysis of the rat optic nerve. *Experimental Neurology, 75*, 525–532.

Garcia-Ayuso, D., Salinas-Navarro, M., Coll-Alcaraz, L., Cánovas-Martínez, I., Bernal-Garro, J. M., Vidal-Sanz, M., et al. (2008). Characterization of the light-sensitive arciform region in the albino rat retina. *Investigative Ophthalmology and Visual Science*, 49 [E-Abstract 4395].

Guillery, R. W. (2002). On counting and counting errors. *Journal of Comparative Neurology, 447*, 1–7.

Jeffery, G. (1985). The relationship between cell density and the nasotemporal division in the rat retina. *Brain Research, 347*, 354–357.

Klöcker, N., Zerfowski, M., Gellrich, N. C., & Bähr, M. (2001). Morphological and functional analysis of imcomplete CNS fiber tract lesion: Gradded crush of the rat optic nerve. *Journal of Neuroscience Methods, 110*, 147–153.

Ko, M. L., Hu, D. N., Ritch, R., Sharma, S. C., & Chen, C. F. (2001). Patterns of retinal ganglion cell survival after brain-derived neurotrophic factor administration in hypertensive eyes of rats. *Neuroscience Letters, 305*, 139–142.

Lafuente López-Herrera, M. P., Mayor-Torroglosa, S., Miralles de Imperial, J., Villegas-Pérez, M. P., & Vidal-Sanz, M. (2002). Transient ischemia of the retina results in altered retrograde axoplasmic transport: neuroprotection with brimonidine. *Experimental Neurology, 178*, 243–258.

Lafuente, M. P., Villegas-Pérez, M. P., Mayor, S., Aguilera, M. E., Miralles de Imperial, J., & Vidal-Sanz, M. (2002). Neuroprotective effects of brimonidine against transient ischemia-induced retinal ganglion cell death: a dose response in vivo study. *Experimental Eye Research, 74*, 181–189.

Lafuente, M. P., Villegas-Pérez, M. P., Sellés-Navarro, I., Mayor-Torroglosa, S., Miralles de Imperial, J., & Vidal-Sanz, M. (2002). Retinal ganglion cell death after acute retinal ischemia is an ongoing process whose severity and duration depends on the duration of the insult. *Neuroscience, 109*, 157–168.

Levkovitch-Verbin, H., Quigley, H. A., Martin, K. R. G., Zack, D. J., Pease, M. E., & Valenta, D. F. (2003). A model to study differences between primary and secondary degeneration of retinal ganglion cells in rats by partial optic nerve transaction. *Investigative Ophthalmology and Visual Science, 44*, 3388–3393.

Linden, R., & Perry, V. H. (1983). Massive retinotectal projection in rats. *Brain Research, 272*, 145–149.

Lund, R. D. (1965). Uncrossed visual pathways of hooded and albino rats. *Science, 149*, 1506–1507.

Lund, R. D. (1969). Synaptic patterns of the superficial layers of the superior colliculus of the rat. *Journal Comparative Neurology, 135*, 179–208.

Lund, R. D., Land, P. W., & Boles, J. (1980). Normal and abnormal uncrossed retinotectal pathways in rats: An HRP study in adults. *Journal Comparative Neurology, 15*, 711–720.

Lund, R. D., Wang, S., Lu, B., Girman, S., Holmes, T., Sauvé, Y., et al. (2007). Cells isolated from umbilical cord tissue rescue photoreceptors and visual functions in a rodent model of retinal disease. *Stem Cells, 25*, 602–611.

Marco-Gomariz, M. A., Hurtado-Montalbán, N., Vidal-Sanz, M., Lund, R. D., & Villegas-Pérez, M. P. (2006). Phototoxic-induced photoreceptor degeneration causes retinal ganglion cell degeneration in pigmented rats. *Journal Comparative Neurology, 498*, 163–179.

Martin, P. R. (1986). The projection of different retinal ganglion cell classes to the dorsal lateral geniculate nucleus in the hooded rat. *Experimental Brain Research, 62*, 77–88.

Mayor-Torroglosa, S., De la Villa, P., Rodríguez, M. E., López-Herrera, M. P., Avilés-Trigueros, M., García-Avilés, A., et al. (2005). Ischemia results 3 months later in altered ERG, degeneration of inner layers, and deafferented tectum: Neuroprotection with brimonidine. *Investigative Ophthalmology Visual Science, 46*, 3825–3835.

McCall, M., Robinson, S. R., & Dreher, B. (1987). Differential retinal growth appears to be the primary factor producing the ganglion cell density gradient in the rat. *Neuroscience Letters, 79*, 78–84.

Métin, C., Irons, W. A., & Frost, D. O. (1995). Retinal ganglion cells in normal hamsters and hamsters with novel retinal projections. I. Number, distribution, and size. *Journal Comparative Neurology, 353*, 179–199.

Mo, X., Yokoyama, A., Oshitari, T., Negishi, H., Dezawa, M., Mizota, A., et al. (2002). Rescue of axotomized retinal ganglion cells by BDNF gene electroporation in adult rats. *Investigative Opthalmology and Visual Science, 43*, 2401–2405.

Nakazawa, T., Tamai, M., & Mori, N. (2002). Brain-derived neurotophic factor prevents axotomized retinal ganglion cell death through MAPK and PI3K signaling pathways. *Investigative Ophthalmology and Visual Science, 43*, 3319–3326.

Park, K. H., Cozier, F., Ong, O. C., & Caprioli, J. (2001). Induction of heat shock protein 72 protects retinal ganglion cells in a rat glaucoma model. *Investigative Ophthalmology and Visual Science, 42*, 1522–1530.

Pavlidis, M., Fischer, D., & Thanos, S. (2000). Photoreceptor degeneration in the RCS rat attenuates dendritic transport and axonal regeneration of ganglion cells. *Investigative Ophthalmology and Visual Science, 41*, 2318–2328.

Peinado-Ramón, P., Salvador, M., Villegas-Pérez, M. P., & Vidal-Sanz, M. (1996). Effects of axotomy and intraocular administration of NT-4, NT-3, and brain-derived neurotrophic factor on the survival of adult rat retinal ganglion cells. *A quantitative in vivo study. Investigative Ophthalmology and Visual Science, 37*, 489–500.

Perry, V. H. (1981). Evidence for an amacrine cell system in the ganglion cell layer of the rat retina. *Neuroscience, 6*, 931–944.

Prusky, G. T., Harker, K. T., Douglas, R. M., & Whishaw, I. Q. (2002). Variation in visual acuity within pigmented, and between pigmented and albino rat strains. *Behavioural Brain Research, 136*, 339–348.

Reese, B. E. (2002). Rat retinal ganglion cell topography. *Investigative Ophthalmology and Visual Science, 43*, 587–594 [Letters for Danias et al.].

Reese, B. E., & Cowey, A. (1986). Large retinal ganglion cells in the rat: Their distribution and laterality of projection. *Experimental Brain Research, 61*, 375–385.

Salinas-Navarro, M., Mayor-Torroglosa, S., Holmes, T., Ortiz, A., Bernal, J. M., Canovas, I., et al. (2005). Automatic quantitative analysis of retinal ganglion cells that project to the superior colliculi in adult Sprague–Dawley rats. *Investigative Ophthalmology and Visual Science*, 46 [E-Abstract 271].

Salinas-Navarro, M., Triviño, A., Ramírez, A. I., Salazar, J. J., Ramírez, J. M., Villegas–Pérez, M. P., et al. (2006). Long term effects of laser-induced ocular hypertension: Retrograde degeneration of retinal ganglion cells. *Investigative Ophthalmology and Visual Science*, 47. E-Abstract 1560.

Sasaki, H., Coffey, P., Villegas-Perez, M. P., Vidal-Sanz, M., Young, M. J., Lund, R. D., et al. (1996). Light induced EEG desynchronization and behavioral arousal in rats with restored retinocollicular projection by peripheral nerve graft. *Neuroscience Letters, 218*, 45–48.

Sauvé, Y., Girman, S. V., Wang, S., Keegan, D. J., & Lund, R. D. (2002). Preservation of visual responsiveness in the superior colliculus of RCS rats after retinal pigment epithelium cell transplantation. *Neuroscience, 114*, 389–401.

Sauvé, Y., Girman, S. V., Wang, S., Lawrence, J. M., & Lund, R. D. (2001). Progressive visual sensitivity loss in the Royal College of Surgeons rat: perimetric study in the superior colliculus. *Neuroscience, 1*, 51–63.

Schnebelen, C., Salinas-Navarro, M., Acar, N., Pasquis, B., Creuzot-Garcher, C. P., Villegas-Pérez, M. P., et al. (2007). Time course of IOP elevation, electroretinographic changes and retinal ganglion cell loss in a rat model of glaucoma induced by laser. *Investigative Ophthalmology and Visual Science*, 48 [E-Abstract 206].

Schnebelen, C., Salinas-Navarro, M., Acar, N., Pasquis, B., Creuzot-Garcher, C. P., Villegas-Pérez, M. P., et al. (2008). Effect of dietary Omega-3 and Omega-6 fatty acids on IOP elevation, electroretinographic changes and retinal ganglion cell loss in a laser-induced rat model of glaucoma. *Investigative Ophthalmology and Visual Science*, 49 [E-Abstract 5499].

Schober, W., & Gruschka, H. (1977). Retinal ganglion cells of the albino rat: A qualitative and quantitative study. *Zeitschrift fur Zellforschung undmikroskopische Anatomie, 91*, 397–414.

Schuettauf, F., Naskar, R., Vorwerk, C. K., Zurakowski, D., & Dreyer, E. B. (2000). Ganglion cell loss after optic nerve crush mediated through AMPA-kainate and NMDA receptors. *Investigative Ophthalmology and Visual Science, 4*, 4313–4316.

Sellés-Navarro, I., Villegas-Pérez, M. P., Salvador-Silva, M., Ruiz-Gómez, J. M., & Vidal-Sanz, M. (1996). Retinal ganglion cell death after different transient periods of pressure-induced ischemia and survival intervals. A quantitative in vivo study. *Investigative Ophthalmology and Visual Science, 37*, 2002–2014.

Siu, A. W., Leung, M. C., To, C. H., Siu, F. K., Ji, J. Z., & So, K. F. (2002). Total retinal nitric oxide production is increased in intraocular pressure-elevated rats. *Experimental Eye Research, 75*, 401–406.

Stone, J. (1983). *Parallel processing in the visual system*. New York: Plenum Press.

Swanson, K. I., Schlieve, C. R., Lieven, C. J., & Levin, L. A. (2005). Neuroprotective effect of sulphydryl reduction in a rat optic nerve crush model. *Investigative Ophthalmology and Visual Science, 46*, 3737–3741.

Thanos, S., Mey, J., & Wild, M. (1993). Treatment of the adult retina with microglia-suppressing factors retards axotomy-induced neuronal degradation and enhances axonal regeneration in vivo and in vitro. *Journal of Neuroscience, 13*, 455–466.

Vidal-Sanz, M., Avilés-Trigueros, M., Whiteley, S. J., Sauvé, Y., & Lund, R. D. (2002). Reinnervation of the pretectum in adult rats by regenerated retinal ganglion cell axons: anatomical and functional studies. *Progress in Brain Research, 137*, 443–452.

Vidal-Sanz, M., Bray, G. M., Villegas-Pérez, M. P., Thanos, S., & Aguayo, A. J. (1987). Axonal regeneration and synapse formation in the superior colliculus by retinal ganglion cells in the adult rat. *Journal of Neuroscience, 7*, 2894–2909.

Vidal-Sanz, M., De la Villa, P., Avilés-Trigueros, M., Mayor-Torroglosa, S., Salinas-Navarro, M., Alarcón-Martínez, L., et al. (2007). Neuroprotection of retinal ganglion cell function and their central nervous system targets. *Eye, 21*, S42–S45.

Vidal-Sanz, M., Lafuente, M. P., Mayor, S., Miralles de Imperial, J., & Villegas-Pérez, M. P. (2001). Retinal ganglion cell death induced by retinal ischemia: Neuroprotective effects of two alpha-2 agonists. *Survey of Ophthalmology, 45*, 261–267.

Vidal-Sanz, M., Lafuente, M., Sobrado-Calvo, P., Selles-Navarro, I., Rodriguez, E., Mayor-Torroglosa, S., et al. (2000). Death and neuroprotection of retinal ganglion cells after different types of injury. *Neurotoxicity Research, 2*, 215–227.

Vidal-Sanz, M., Salinas-Navarro, M., Jiménez-López, M., Valiente-Soriano, F. J., García-Ayuso, D., Bernal, J. M., et al. (2007). Spatial distribution and quantitative análisis of retinal ganglion cells in adult albino rodents. *Investigative Ophthalmology and Visual Science*, 48 [E-Abstract 134].

Vidal-Sanz, M., Villegas-Pérez, M. P., Bray, G. M., & Aguayo, A. J. (1988). Persistent retrograde labeling of adult rat retinal ganglion cells with the carbocyanine dye dil. *Experimental Neurology, 102*, 92–101.

Vidal-Sanz, M., Villegas-Pérez, M. P., Bray, G. M., & Aguayo, A. J. (1993). The use of peripheral nerve grafts to study regeneration after CNS injury. *Neuroprotocols, 3*, 29–33.

Villegas-Pérez, M. P., Aguilera, M. E., Salinas-Navarro, M., Mayor-Torroglosa, S., Holmes, T., Bernal, J. M., et al. (2006). Retinal ganglion cells in adult albino and pigmented rats: Spatial distribution and quantitative analysis. *Investigative Ophthalmology and Visual Science*, 47 [E-Abstract 3318].

Villegas-Pérez, M. P., Lawrence, J. M., Vidal-Sanz, M., Lavail, M. M., & Lund, R. D. (1998). Ganglion cell loss in RCS rat retina: A result of compression of axons by contracting intraretinal vessels linked to the pigment epithelium. *Journal of Comparative Neurology, 392*, 58–77.

Villegas-Pérez, M. P., Vidal-Sanz, M., Bray, G. M., & Aguayo, A. J. (1988). Influences of peripheral nerve grafts on the survival and regrowth of axotomized retinal ganglion cells in adult rats. *Journal of Neuroscience, 8*, 265–280.

Villegas-Pérez, M. P., Vidal-Sanz, M., & Lund, R. D. (1996). Mechanism of retinal ganglion cell loss in inherited retinal dystrophy. *Neuroreport, 7*, 1995–1999.

Villegas-Pérez, M. P., Vidal-Sanz, M., Rasminsky, M., Bray, G. M., & Aguayo, A. J. (1993). Rapid and protracted phases of retinal ganglion cell loss

follow axotomy in the optic nerve of adult rats. *Journal of Neurobiology, 24*, 23–36.

Whiteley, S. J., Sauvé, Y., Avilés-Trigueros, M., Vidal-Sanz, M., & Lund, R. D. (1998). Extent and duration of recovered pupillary light reflex following retinal ganglion cell axon regeneration through peripheral nerve grafts directed to the pretectum in adult rats. *Experimental Neurology, 154*, 560–572.

Williams, R. W., Strom, R. C., Rice, D. S., & Goldowitz, D. (1996). Genetic and environmental control of variation in retinal ganglion cell number in mice. *Journal of Neuroscience, 16*, 7193–7205.

WoldeMussie, E., Ruiz, G., Wijono, M., & Wheeler, L. A. (2001). Neuroprotection of retinal ganglion cells by brimonidine in rats with laser-induced chronic ocular hypertension. *Investigative Ophthalmology and Visual Science, 42*, 2849–2855.